Statistical model for self-assembly of trimesic acid molecules into homologous series of flower phases

A. Ibenskas and E. E. Tornau*

Semiconductor Physics Institute, Center for Physical Sciences and Technology, A. Goštauto 11, LT-01108, Vilnius, Lithuania

(Received 3 July 2012; revised manuscript received 2 October 2012; published 16 November 2012)

The statistical three-state model is proposed to describe the ordering of triangular TMA molecules into flower phases. The model is solved on a rescaled triangular lattice, assuming following intermolecular interactions: exclusion of any molecules on nearest neighbor sites, triangular trio H-bonding interactions for molecules of the same orientation on next-nearest neighbor sites, and dimeric H-bonding interactions for molecules of different ("tip-to-tip") orientations on third-nearest neighbor sites. The model allows us to obtain the analytical solution for the ground state phase diagram with all homologous series of flower phases included, starting with the honeycomb phase ($n = 1$) and ending with the superflower structure ($n = \infty$). Monte Carlo simulations are used to obtain the thermodynamical properties of this model. It is found that phase transitions from disordered to any of the flower phases (except $n = 1$) undergo via intermediate correlated triangular domains structure. The transition from the disordered phase to the intermediate phase is, most likely, of the first order, while the transition from the intermediate to the flower phase is definitely first order phase transition. The phase diagrams including low-temperature flower phases are obtained. The origin of the intermediate phase, phase separation, and metastable structures are discussed.

DOI: 10.1103/PhysRevE.86.051118 PACS number(s): 64.60.De, 64.75.Yz, 75.10.Hk

I. INTRODUCTION

Self-assembly of molecular structures on surfaces is usually caused by weak noncovalent (van der Waals, capillary, π-π, or H bond) intermolecular interactions. Precise and controlled application of intermolecular forces makes possible to obtain ordered supramolecular architectures on very small length scales. The ability to tune the pattern of such two-dimensional structures by external experimental parameters, such as temperature, molecular concentration, and even size and shape of a molecule, is the ultimate goal [1] of all ongoing experimental and theoretical studies.

Apart from purely scientific interest, self-assembled monolayers are successfully applied in different fields of molecular electronics and nanobiomedicine. Thus, individual molecular layers have been proposed as active elements of molecular electronic logic and memory devices [2,3] and used for information [4] and high-density data storage [5]. Self-assembled monolayers are applied in molecular photodevices [6] and for efficient photocurrent generation [7] and construction of gas sensors [8]. They can increase power density of the methanol fuel cells [9] and be used as lubricants and for protective coating [10]. Certain forms of alkanethiols self-assembled on gold and silver might be used to study the interaction of synthetic materials with biologically relevant systems [11,12]. Molecular arrays of organic molecules of trimesic acid (TMA), as well as some other similar (TPA, TMLA and TDA) molecules, represent templates for handling and organization of functional species, particularly C60 [13,14].

The properties of cooperativity, selectivity, and directionality make the H bonds extremely useful assembling element of supramolecular structures. One of the most popular motifs found in supramolecular assembly of H-bonded molecular arrays is a two-dimensional honeycomb pattern, which might be obtained by combining triangular [15–17], elongated [18,19], or mixed triangular and elongated [20] molecular building blocks. Very interesting two-dimensional molecular networks are composed of organic TMA molecules [14,21–28]. TMA is a simple molecule of a strict triangular form composed of three carboxyl acid groups ordered in a planar triangular arrangement around the central phenyl ring. The carboxylic acid groups at the vertices of the triangle allow the molecule to act as a hydrogen-bonding unit and create porous honeycomb and other ordered molecular networks.

The homologous series of flower phases (Fig. 1), of which the honeycomb phase is the first member in a row, is the most fascinating sequence of self-assemblies built by TMA molecules. All this sequence might be defined by the index n. Increase of n corresponds to increase of a distance between the centers of neighboring hexagons (or unit cell of the structure). For the last member of this series, the superflower phase ($n = \infty$), this distance would be infinity, and the unit cell of this phase is a rhombus connecting centers of four neighboring molecules. The flower structures have threefold symmetry, and all carboxylic acid vertices are engaged in dimeric and/or trimeric H bonding. Honeycomb phase ($n = 1$) is characterized by a dimeric ("tip-to-tip") H-bonding only. With further increase of n the number of dimeric bonds decreases and trimeric increases. The flower phases with $n > 1$ have both dimeric and trimeric motives, except for $n = \infty$, which is characterized by trimeric H bonding only.

The flower phases of TMA molecules are obtained either at ultra-high vacuum (UHV) conditions [honeycomb phase on Cu(100) [26], Au(111) [27] and the series up to $n = 8$ and $n = \infty$ on Au(111) [28]] or on solid-liquid interface by tuning an appropriate concentration of solvent fat acids on highly ordered pyrolytic graphite (honeycomb and flower $n = 2$ phase [21–23] and fragments of superflower phase with alcohols [14]). The most interesting STM experiment demonstrating the almost all homologous sequence of such phases was performed by Ye *et al.* [28].

Statistical models, which make possible to determine the stability limits of ordered structures, are successfully

*et@et.pfi.lt

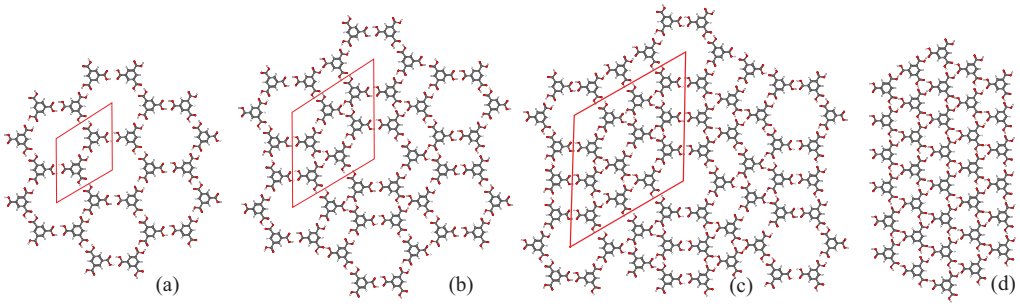

FIG. 1. (Color online) Schematic view of homologous series of flower phases formed by triangular TMA molecules: (a) honeycomb phase ($n = 1$) with dimeric interactions only; (b) flower ($n = 2$) and (c) second-generation flower phase ($n = 3$) with both dimeric and trimeric interactions; (d) superflower phase ($n = \infty$) with trimeric interactions only. Unit cell in (a)–(c) is shown by a gray (red in electronic version) rhombus connecting the centers of hexagons.

employed for adatoms on surfaces. They are less popular for simulation of ordering of molecular structures as due to large sizes of molecules as well as complicated and sometimes even exotic conformations, which makes it difficult to unambiguously choose the appropriate intermolecular interactions. Nevertheless, the models used for liquid crystals [29], polymers [30], proteins [31], or colloid particles [32,33] are now applied for description of self-assembling molecular systems [16,20,34,35]. These models are more advanced forms of the two-state Ising or lattice-gas models and frequently their extensions to larger number of states, since ordering molecular species tends to demonstrate multiorientational behavior. The molecules are reduced to rather simple geometrical shapes and orientations on a lattice, and the dynamics of molecular ordering is governed by defined interaction rules. The simulation of these models allows one to predict the phase diagrams and growth dynamics of different self-assembled molecular structures.

In this paper the statistical model for ordering of triangular TMA molecules into homologous series of flower phases is presented. Our model is based on experimental observation [21–23,28] that the self-assembly of TMA molecules into flower phases is caused by two types of H-bond intermolecular interactions: the dimeric interactions of two molecules of different orientations and the trimeric interactions of three molecules of the same orientation. To simplify the model, we assume the dimeric interactions act between a pair of molecules separated by third-nearest neighbor (3NN) distances of triangular lattice and trimeric interactions among a trio of molecules separated by next-nearest neighbor (2NN) distances. The proposed model is the three-state model: The two states differ in 60-degree rotation around the center of the molecule, and the third state is the vacancy state. The model makes possible to obtain a rich phase diagram of flower phases and captures the essential properties of a larger-scale (experimental) behavior. By using this model, we obtain analytical expressions for ground state energies of homologous series of flower phases and determine thermodynamical properties of these phases by Monte Carlo (MC) simulations.

II. MODEL

A statistical model for description of homologous series of flower phases might be defined on an original Au(111) lattice (with lattice constant a_{Au}), since a matrix transformation between the lattice vectors of the honeycomb TMA structure ($n = 1$) and Au(111) is known [27]. In this case the distance between the centers of two adjacent TMA molecules would correspond to $2\sqrt{3}a_{\mathrm{Au}}$, which is the sixth nearest neighbor (6NN) distance of the original triangular Au(111) lattice.

The flower phases with $n > 1$ were not identified in experiment [27], but the packing density of the honeycomb phase in this experiment (0.8 mol/nm^2) was just 6% smaller than that obtained in experiment [28], where other flower phases were found. Thus, it is quite reasonable to assume that the trio H-bond interaction (vital for formation of flower phases with $n > 1$) might be important when three molecules form an equilateral triangle with the sides equal to $3a_{\mathrm{Au}}$. This distance corresponds to a 5NN distance of initial Au(111) lattice.

Still, for statistical models, with particles moving over the sites of the lattice, such long (5NN and 6NN) distances are rather inconvenient. Therefore we propose the scaling of the underlying lattice as shown in Fig. 2. The number of sites for molecule movement decreases under such transformation, but

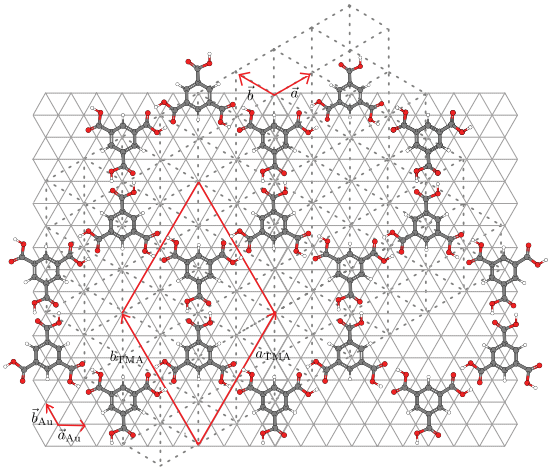

FIG. 2. (Color online) Scaling of the underlying lattice for TMA molecules. The TMA system in a honeycomb phase on Au(111) is transformed to the same system on a new underlying lattice with distance between the TMA molecules $2a = 2a_{\mathrm{Au}}\sqrt{3}$. This distance is 6NN distance of a triangular lattice on Au(111) and corresponds to 3NN distance of a new lattice.

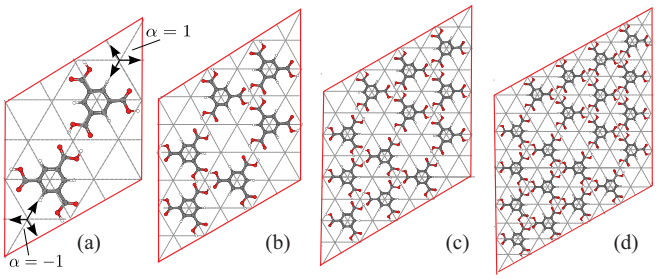

FIG. 3. (Color online) Unit cells of (a) honeycomb ($n = 1$), (b) flower ($n = 2$), (c) second-generation flower ($n = 3$), and (d) third generation flower phases in a 2NN-3NN model on a new underlying triangular lattice. Molecule arrangements in (a) might be an illustration of two states of the molecule (top molecule, $s_i = 1$, and bottom molecule, $s_i = -1$). Bond vectors ($\alpha = \pm 1$) are also shown in (a) by black arrows.

the distance between the centers of two TMA molecules in a honeycomb phase is just $2a$, which is the 3NN distance of a new lattice. The distance between the molecules of a triangle forming trimeric H bonds corresponds just to 2NN distance of a new lattice, $a\sqrt{3}$.

Thus, we propose the three-state model on triangular lattice with lattice constant $a = \sqrt{3}a_{\mathrm{Au}}$. Two states of the molecule, corresponding to variable $s_i = \pm 1$, are shown in Fig. 3(a). The variable is defined on a lattice site i, where the center of the molecule resides. These states differ in 60-degree rotation of the molecule and correspond to two orientations encountered in a honeycomb phase (and all other flower phases) of TMA molecules. The third state, $s_i = 0$, is the vacancy state. Such choice of nonzero states defines the dimeric H bond of two molecules at 3NN distances, if the orientations (states) of these molecules are different. In contrast to two-state models, in this model there might be two different "antiferromagnetic" $(+1 \cdots -1)$ orientations of triangular molecules [32,35]. One corresponds to dimeric H-bond "tip-to-tip" intermolecular orientation, shown in Fig. 3(a), and we denote its interaction energy as ϵ_1. The other corresponds to "side-to-side" orientation, and we assume its interaction energy to be zero. Strictly, the pair energy $v^{3\mathrm{NN}}(s_i,s_j;\alpha)$ depends on the direction of the connecting lattice (bond) vectors $\alpha = \pm 1$ shown in Fig. 3(a). The only nonzero pair energies in our model are $v^{3\mathrm{NN}}(1,-1;1) = \epsilon_1$ for directions corresponding to $\alpha = 1$ and $v^{3\mathrm{NN}}(-1,1;-1) = \epsilon_1$ for directions corresponding to $\alpha = -1$.

In our model the trio interaction ϵ_t might be created if three molecules of the same nonzero state (either $s = 1$ or $s = -1$) form a common triangle and the carboxylic acid vertex of each of the molecule is directed to the center of this triangle. This is the way TMA molecules residing on 2NN distances in between form the trimeric H bond [see Figs. 3(b)–3(d)]. However, the pair energy of two molecules separated by 2NN distance is assumed to be zero as well as pair energies of molecules at distances exceeding 3NN distance. The location of two molecules at the nearest neighbor (1NN) sites is forbidden due to the large size of the molecules (infinite repulsion, i.e., exclusion). Thus, the model is defined by dimeric and trimeric H-bond interactions for intermolecular distances corresponding to 3NN and 2NN distances of a triangular lattice, respectively. In general, our "diluted" Hamiltonian might be written in a form

$$\mathcal{H} = -\frac{1}{2}\sum_{\alpha}\sum_{\{i,j\}_\alpha} v^{3\mathrm{NN}}(s_i,s_j;\alpha) - \frac{1}{3}\epsilon_t \sum_{i,j,k} \delta^{2\mathrm{NN}}(s_i,s_j,s_k) + \mu\sum_i s_i^2. \tag{1}$$

Here the first sum is defined on 3NN distances and all $v^{3\mathrm{NN}}(s_i,s_j;\alpha) = 0$, except $v^{3\mathrm{NN}}(1,-1;1) = v(-1,1;-1) = \epsilon_1$. The second sum is defined on 2NN distances, and $\delta^{2\mathrm{NN}}(s_i,s_j,s_k)$ is equal to 1 when $s_i = s_j = s_k = 1$ or $s_i = s_j = s_k = -1$ and carboxylic vertices are directed to the center of a common triangle, and zero otherwise, including the case $\delta^{2\mathrm{NN}}(0,0,0) = 0$. Namely, the neglect of the term with all zero states distinguishes the second term from the usual three-state ferromagnetic Potts model and $\delta^{2\mathrm{NN}}(s_i,s_j,s_k)$ from the three-state Kroeneker delta-type function $\delta(s_i,s_j,s_k)$. The vacancy states exist, but have no effect to intermolecular energies. Only at $\mu \to -\infty$, when the model (1) reaches the, so-called, Ising limit (two-state model, no vacancy state), $\delta^{2\mathrm{NN}}(s_i,s_j,s_k) = \delta(s_i,s_j,s_k)$. The third term introduces different molecular concentration, and μ denotes the chemical potential.

III. GROUND STATE ENERGIES

In our 2NN-3NN model the ground state energies of the three main phases (honeycomb $n = 1$, flower $n = 2$, and superflower $n = \infty$) are

$$\begin{aligned} E_1 &= -c_1\left(\tfrac{3}{2}\epsilon_1 - \mu\right), \\ E_2 &= -c_2\left(\epsilon_1 + \tfrac{1}{3}\epsilon_t - \mu\right), \\ E_\infty &= -c_\infty(\epsilon_t - \mu), \end{aligned} \tag{2}$$

where as a measure of phase concentration we choose the coverage of lattice sites occupied by the center of TMA molecule. Therefore we can write $c_1 = c_{\mathrm{hon}} = 1/6$, $c_2 = c_{\mathrm{fl}} = 2/9$, and $c_\infty = c_{\mathrm{sfl}} = 1/3$. In a similar way we can write the ground state energies of other flower phases with $n > 2$. Actually, for a 2NN-3NN model it is possible to find the analytical expression for these energies as a function of n in a form

$$E_n = -c_n\left(\frac{3}{n+1}\epsilon_1 + \frac{n-1}{n+1}\epsilon_t - \mu\right), \tag{3}$$

where $c_n = \frac{n}{3(n+1)}$. The phase diagram represents an infinite set of $E(n) = E(n-1)$ lines in ϵ_t/ϵ_1 and μ/ϵ_1 coordinates (see Fig. 4). With increase of n each line intercepts a smaller interval of μ/ϵ_1, and the range of values at which the n-th phase exists decreases. At large n the region of n-th phase existence becomes infinitesimally small. The lines coincide at the $\epsilon_t/\epsilon_1 = \mu/\epsilon_1 = 3/2$ point, and this is the largest value of chemical potential when the molecules still exist on a lattice. The most important lines are those which separate honeycomb ($n = 1$) and flower ($n = 2$) phases, $\mu/\epsilon_1 = -\frac{1}{2} + \frac{4}{3}\epsilon_t/\epsilon_1$, and flower and second generation flower ($n = 3$) phases, $\mu/\epsilon_1 = -\frac{5}{4} + \frac{11}{6}\epsilon_t/\epsilon_1$. The general form of the $E(n) = E(n-1)$ line is $\mu/\epsilon_1 = -A(n) + B(n)\epsilon_t/\epsilon_1$, where $A(n) = \frac{3(n^2-n-1)}{n(n+1)}$ and $B(n) = \frac{3n^2-n-2}{n(n+1)}$. Thus, the superflower phase would exist when $n \to \infty$ and $\mu/\epsilon_1 < -3 + 3\epsilon_t/\epsilon_1$.

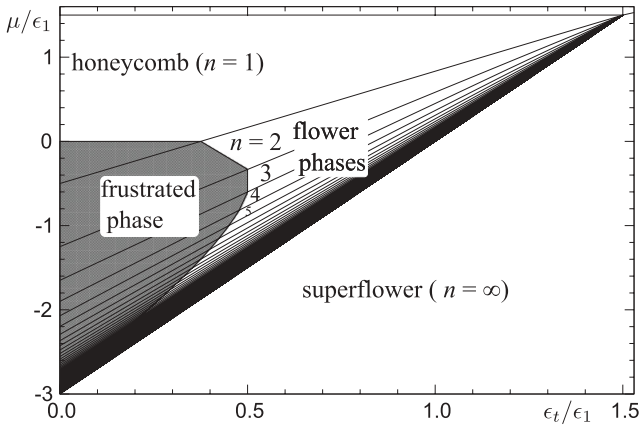

FIG. 4. Ground state phase diagram of flower phases.

There is one phase in this model which has lower energy than the flower phases at low values of ϵ_t/ϵ_1. This is the phase frustrated on 3NN distances. The ϵ_1 is just one of $(+1\cdots-1)$-type of interactions bonding inequivalent nonzero orientations. It corresponds to "tip-to-tip" H bonding in chemical terms or antiferromagnetic interaction in magnetic terms. Two other bonding types of triangular molecules with interacting vertices are also conceivable on 3NN sites [25,35]. They correspond to "tip-to-side" (ferromagnetic) interaction of two molecules of the same nonzero orientation and side-to-side (antiferromagnetic) interaction of two molecules of different nonzero orientation. We neglect them in our model. Still, at negative values of chemical potential μ, when concentration increases, many more molecules start to appear at the centers of hexagons, i.e., at 3NN distance from the nearest molecules forming the honeycomb ring. Frustration on 3NN distances is observed at the Ising limit of the three-state model when it transforms into the two-state model (no zero state), when all hexagon centers are occupied. Actually, at that concentration we have the situation equivalent to the nearest-neighbor antiferromagnetic Ising model on a triangular lattice, which has the frustrated phase as the ground state. The only difference here is that at $\epsilon_t/\epsilon_1 = 0$ we have the frustrated phase on 3NN distances. The ground state energy of this phase can be easily expressed as

$$E_{\rm fr} = -c_{\rm fr}(\epsilon_1 - \mu), \tag{4}$$

and the concentration, $c_{\rm fr} = 1/4$, comes from filling of the third (zero) sublattice of the honeycomb phase (2). Equating this expression to the energy of each of flower phases (3) we obtain the set of lines separating frustrated and flower phases. They are $\mu/\epsilon_1 = \frac{n-1}{(3-n)(n+1)}[3(n-1) - 4n\frac{\epsilon_t}{\epsilon_1}]$, except for $n = 3$ when the line is $\epsilon_t/\epsilon_1 = 0.5$. The frustrated phase is shaded gray in Fig. 4.

IV. SIMULATION RESULTS

The thermodynamics of this model was simulated by the MC method. We used the Metropolis algorithm and the, so-called, Glauber dynamics. The calculation procedure was the following: (1) the sites of triangular lattice were occupied with molecules in states $+1$, -1, and 0, i.e., the lattice was filled with molecular concentration c (defined as the coverage of sites occupied by the center of TMA molecule) corresponding to some fixed chemical potential μ; (2) the molecule was chosen randomly and its initial energy E_1 was calculated; (3) the initial state of that molecule was changed (with equal probability) to one of two remaining states, and the final energy E_2 was calculated; (4) the new state was accepted, if the energy difference $\Delta E = E_2 - E_1 < 0$, or accepted with the probability $\sim\exp(-\Delta E/kT)$, if $\Delta E > 0$. Using this type of dynamics the molecular concentration was changed at fixed chemical potential. Using the, so-called, Kawasaki dynamics the concentration is fixed, and the molecule chosen randomly makes jumps from one site to another with the probability $\sim\exp(-\Delta E/kT)$. Glauber dynamics is very convenient for description of statical properties of ordering systems and less time consuming than the Kawasaki dynamics.

For calculations we used the triangular lattices of sizes $L = N \times N$ with N from $48\sqrt{3}$ up to $96\sqrt{3}$ with periodic boundary conditions. Most calculations for small $n = 1$–3 were performed on a former lattice. We have chosen this lattice as the optimal, i.e., further increase of the lattice size over the optimal one does not essentially change the phase transition temperature.

To choose the optimal work regime and accuracy of simulation, we varied the limiting number of MC steps per site (MCS) up to 10^7. Except a very narrow range of temperatures related to a first-order phase transition point from intermediate-to-flower phase, T_{c2}, for all other ranges of temperature the MCS limit, 5×10^5–10^6, was quite sufficient to stabilize the energy minimum (at that particular temperature). For the particular range around T_{c2} we could use two simulation scenarios: either take around 10^7 MCS (a bit better accuracy, but longer computations) or take around 2×10^6 MCS (obtained as a reasonable estimate), perform several independent runs, and average over these runs. We have chosen the latter way and took five independent runs for averaging, which, for small $n < 4$, were performed on a $N = 48\sqrt{3}$ lattice. Thus, the accuracy in our calculation of this transition point is determined by a spread of results used for averaging, and error bars do not exceed ± 0.01 for $k_B T_{c2}/\epsilon_1$. The accuracy of results for the phase transition point from disordered to $n = 1$ phase ($k_B T_c/\epsilon_1$) and from disordered to intermediate phase ($k_B T_{c1}/\epsilon_1$) was determined by the temperature step of our calculations (mostly ± 0.002).

For main calculations we have chosen the ratio of interaction constants $\epsilon_t/\epsilon_1 = 1.2$. This value is related to calculated H-bond interactions for dimers and trimers of benzoic acid and TMA molecules. According to gas-phase density functional theory calculations [23], the H-bonding enthalpy in cyclic dimer and cyclic trimer of benzoic acid is -20.4 and -26.2 kcal/mol, respectively; i.e., H bonds in the dimer are 1.5 kcal/mol stronger than in the trimer. It should be noted that similar values are obtained using gas-phase semiempirical MOPAC calculations [36]: The values of H-bonding enthalpies for dimer and trimer are, respectively, equal to -20.867 and -24.45 kcal/mol for benzoic acid and -20.3 and -25.2 kcal/mol for TMA molecules [37]. Though the magnitudes of interactions in all gas-phase calculations might be overestimated, the ratio of ϵ_t/ϵ_1 is quite reasonable.

The ground state calculations give the following limits for flower phases at $\epsilon_t/\epsilon_1 = 1.2$: $\mu/\epsilon_1 > 1.1$ $(n = 1)$, $0.95 < \mu/\epsilon_1 < 1.1$ $(n = 2)$, $0.87 < \mu/\epsilon_1 < 0.95$ $(n = 3)$,

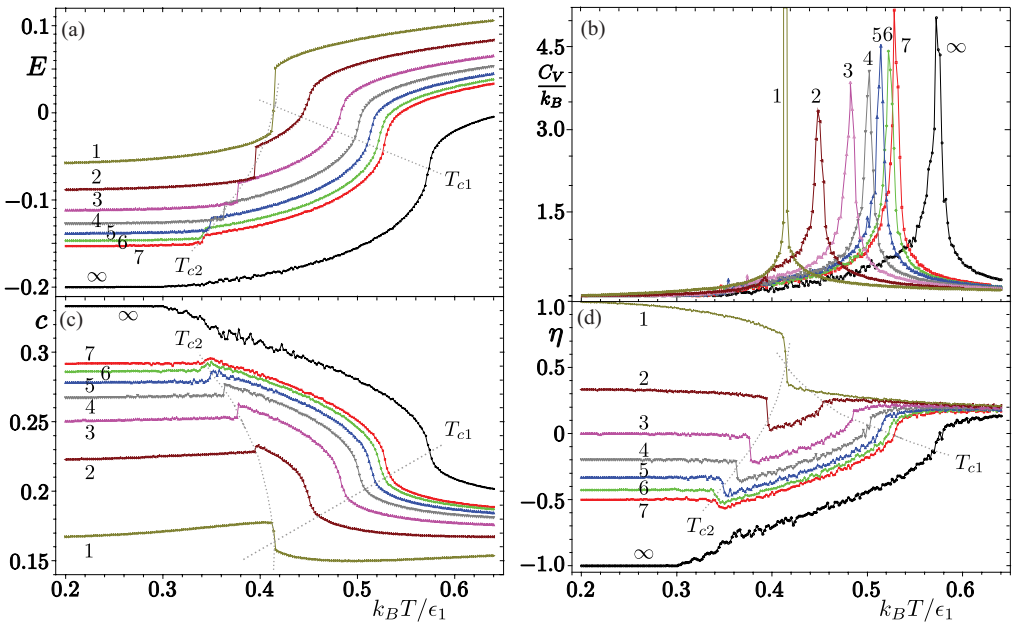

FIG. 5. (Color online) Temperature dependencies of (a) average energy, (b) specific heat, (c) concentration, and (d) order parameter for flower phases $n = 1$ ($\mu/\epsilon_1 = 1.15$), 2 ($\mu/\epsilon_1 = 1$), 3 ($\mu/\epsilon_1 = 0.9$), 4 ($\mu/\epsilon_1 = 0.84$), 5 ($\mu/\epsilon_1 = 0.8$), 6 ($\mu/\epsilon_1 = 0.77$), 7 ($\mu/\epsilon_1 = 0.75$), and superflower phase $n = \infty$ ($\mu/\epsilon_1 = 0.6$) obtained for $L = [(48 - 50)\sqrt{3}]^2$ lattices. Dashed curves in (a), (c), and (d) mark the phase transition temperature points. The peaks in (b) indicate the T_{c1} point.

$0.82 < \mu/\epsilon_1 < 0.87$ ($n = 4$), $0.786 < \mu/\epsilon_1 < 0.82$ ($n = 5$), etc. The transition to the superflower phase $n \to \infty$ is at $\mu/\epsilon_1 \leqslant 0.6$. Further, by using the term "$n = \cdots$ phase region" we refer to the ranges of μ, where according to the ground state calculation that particular phase n has to occur at low temperature.

We calculated the temperature dependencies of some important functions characterizing the phase transition points at different values of chemical potential. These functions are average energy, $E = \langle\mathcal{H}\rangle/L$, dimensionless specific heat, $C_v/k_B = (\langle\mathcal{H}^2\rangle - \langle\mathcal{H}\rangle^2)/L(k_BT)^2$, concentration, $c = \sum_i s_i^2/L$, and phase order parameter. The last is defined as the average number of certain molecules surrounding each molecule and was obtained from the formula

$$\eta_n = \tfrac{1}{3}N_{3NN} - \tfrac{1}{6}N_{2NN}, \qquad (5)$$

where N_{3NN} is the average number of tip-to-tip (antiferromagnetic) neighbors at 3NN distance and N_{2NN} is the average number of second nearest neighbors of the same (ferromagnetic) orientation satisfying the trimeric bond condition. The coefficients are chosen in such a way that for ideal honeycomb and superflower phases $\eta_1 = 1$ and $\eta_\infty = -1$, respectively. Correspondingly, for ideal flower phases, $\eta_2 = 1/3$, $\eta_3 = 0$, $\eta_4 = -1/5$, $\eta_5 = -1/3$, etc., or generally $\eta_n = \frac{3-n}{n+1}$.

Temperature dependencies of main functions, characterizing phase transition points obtained for different flower phases by MC calculations, are presented in Fig. 5. The curves were obtained by increasing temperature starting from an ideal phase (which in accordance with the ground state results has to occur at that particular value of chemical potential μ) and at each new temperature step taking the configuration obtained at a previous step.

We found that the transition from the $n = 1$ to disordered phase at T_c is the direct transition. For other flower phases the transition from flower to disordered phase is mediated by a correlated triangular domains structure which we further call the intermediate (I) phase. This phase exists between the phase transition points T_{c1} (disordered−I phase) and T_{c2} (I-phase−flower phase). In comparison to disordered phase, this phase has strong correlations corresponding to ϵ_1 and ϵ_t bonding, but no regular flower structure. The I-phase structure is characterized by triangular domains of trimerically bonded molecules of one orientation separated (usually by dimeric bonds) from triangular domains of molecules of another orientation. Contrary to ordering in ideal flower phases, the I-phase pattern does not show well-defined long-range order, except for some temperature regions above the $n = 2$ phase which are close to $n = 1$ region. An essential feature of the flower phases is the nicely ordered set of honeycomb hexagons which are found at the angles of a unit cell of Fig. 3. Thus, the I phase usually has a very small number of regular tip-to-tip hexagons, except for the mentioned region above the $n = 2$ phase, where small honeycomb domains might be seen.

The specific heat C_v at T_c and T_{c1} has very nice peak [Fig. 5(b)]. The C_v at T_{c2} has a small "hump" discernible for transitions into phases with small index $n(<4)$, but hardly visible for those with higher n.

Here we describe the transitions to some of flower phases in more detail.

A. $n = 1 - 2$ phase region

The $n = 1$ and $n = 2$ phases are most popular flower structures of the series. They both were experimentally obtained at UHV conditions on Au(111) [28] and graphite [14,21,22]. The honeycomb phase was also found in other experiment on Au(111) [27] and in a slightly distorted form on Cu(100) [26]. These two phases are characterized by the simplest symmetry

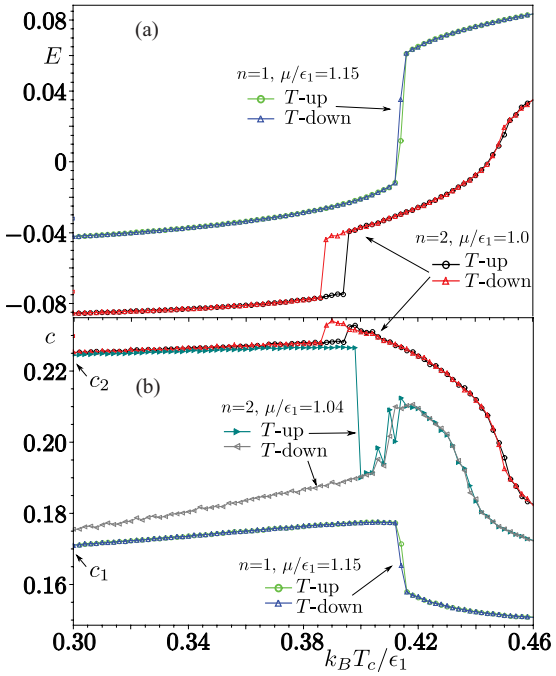

FIG. 6. (Color online) Temperature dependencies of (a) average energy and (b) concentration in $n = 1$ and 2 phase regions obtained using runs with increasing (T-up) and decreasing (T-down) temperature. The energy curves of $n = 1$ region are shifted up by 0.01 for clarity.

in comparison to other flower phases and therefore are most easily accessible in both simulations with increasing as well as decreasing temperature (i.e., in simulation starting from high-temperature random structure). In Fig. 6 we demonstrate temperature dependences of energy and concentration for both types of simulation.

In the $n = 1$ phase region the energy has a jump at transition point $T_c = T_{c1} = T_{c2}$ that implies first order phase transition. It is interesting to note that this jump is observed even for small lattices. This makes this transition a bit different from such typical first-order phase transitions, as the 10-state Potts model [38,39] or modified XY model [40], which demonstrate the steepening of $E(T)$ dependence at T_c with increase of lattice size $L = N^2$. Possibly this difference is a manifestation of a very strong first order phase transition in our model, caused by proximity of the honeycomb-gas phase separation experienced by the system at low concentration of molecules. However, temperature hysteresis in our calculations of T_c to $n = 1$ phase is almost negligible. The transition temperature T_c demonstrates linear behavior, $T_c(N) - T_c(\infty) \sim N^{-2}$, as observed for the first order phase transitions [38,40].

We obtain two phase transitions in the $n = 2$ phase region. The high-temperature phase transition at T_{c1} from disordered to I phase is characterized by a continuous $E(T)$ dependence and a peak of specific heat. The low-temperature phase transition from I phase to $n = 2$ phase is characterized by energy and concentration jumps and small hysteresis at T_{c2}.

The transition at T_{c2} is rather similar to the disordered-to-$n = 1$ phase transition at T_c, because of similar (yet smaller) jump in energy. Moreover, the transition temperature $T_{c2}(N)$ demonstrates linear behavior with N^{-2}, which allows one to attribute the transition to the first order phase transitions. However, there are some differences between T_c and T_{c2}. First, the hysteresis is observed at T_{c2}, which is not seen at T_c. Second, the peak of specific heat which exists at T_c is substituted by a small hump at T_{c2}, and, instead, the C_v peak occurs at T_{c1}. Thus, it looks like with decrease of μ (increase of c) for further members of homologous series the transition at T_c splits into two transitions at T_{c1} and T_{c2}, and the I phase is needed as a prerequisite to obtain the flower structure for phases with $n > 1$.

The nature of the phase transition at T_{c1} is, most likely, also of the first order. Though around T_{c1} there is no hysteresis and the $E(T)$ dependence is continuous and steepens rather weakly with N, the $T_{c1}(N)$ is linear with respect of $1/N^2$, and the Binder cumulant, $V_4 = 1 - \langle E^4\rangle/3\langle E^2\rangle^2$, demonstrates a deep minimum in between the value 0.67 (above and below T_{c1}). Certainly more accurate calculations have to be performed in order to unambiguously determine the nature of these phase transitions.

The snapshots in Fig. 7 reveal gradual reconstruction process occurring with decrease of temperature: Below T_{c1} the I phase is obtained [Fig. 7(b)] with some domains of the $n = 1$ structure; with further decrease of temperature a few $n = 2$ domains are created, and such a situation [Fig. 7(c)] is conserved almost up to the transition point at T_{c2}, where the $n = 2$ phase is abruptly established. A similar tendency is seen in concentration dependencies. When temperature-decreasing simulation is used, the system at T_{c2} moves from the I phase straight to an ideal $n = 2$ structure ($c = 2/9 = 0.222$).

One more interesting feature of the $n = 1 - 2$ phase region is the possibility to obtain the phase transition from the $n = 1$ to 2 phase with temperature. In our model this transition occurs at higher temperature inside the $n = 2$ phase region, but close to the $n = 1 - 2$ phase boundary (obtained in ground state calculation at $T = 0$). This calculation demonstrates that the phase boundary is at $\mu/\epsilon_1 = 1.1$. But actually down to as low

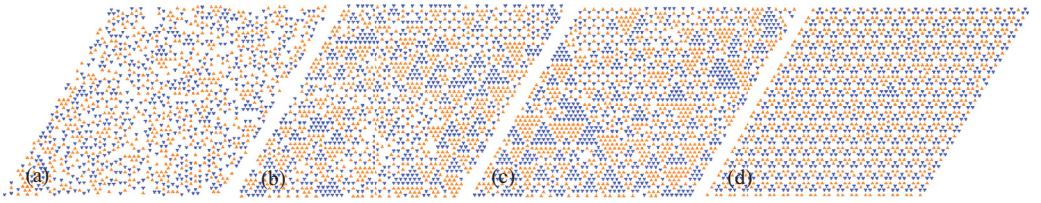

FIG. 7. (Color online) Snapshots at different temperature at $\mu = 1$ ($n = 2$ phase region). Here (a) $k_BT/\epsilon_1 = 0.52$ (disordered phase), (b) 0.43 (I-phase, $T < T_{c1}$), (c) 0.39 (I-phase, but T very close to T_{c2}), and (d) 0.30 ($n = 2$ phase, $T < T_{c2}$). Two states of the molecule are represented by dark and light triangles (blue and orange in electronic version).

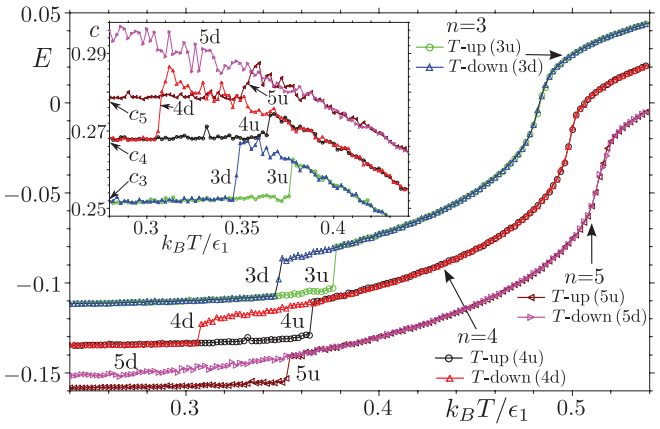

FIG. 8. (Color online) Temperature dependencies of energy and concentration (inset) for $n = 3$ ($\mu/\epsilon_1 = 0.9$), $n = 4$ ($\mu/\epsilon_1 = 0.85$), and $n = 5$ ($\mu/\epsilon_1 = 0.8$) phase regions obtained with increasing (T-up) and decreasing (T-down) temperature. For clarity the energy curves of $n = 4$ and 5 regions are shifted down by 0.01 and 0.02, respectively.

as $\mu/\epsilon_1 = 1$ the $n = 1$ phase is still obtained in simulations with decreasing temperature. In simulations with increasing temperature at $1 < \mu/\epsilon_1 < 1.1$ the transition from the $n = 2$ to the $n = 1$, and only with further increase of T to the I phase, is obtained. The $c(T)$ dependence in this interval of chemical potential is illustrated in Fig. 6(b) by the curve for $\mu/\epsilon_1 = 1.04$.

B. $n = 3 - 5$ phase region

These and some further phases were experimentally found only at UHV conditions on Au(111) [28].

Our results in regions corresponding to those three phases are shown in Fig. 8, and they are qualitatively similar to those obtained in the $n = 2$ phase region. However, with increase of n the size of temperature hysteresis increases, and the ideal structure is no longer so easily accessible for runs with decreasing temperature. In the $n = 3$ phase region the majority of runs successfully reach the ideal structure. In Fig. 8 we demonstrate the successful run into the $n = 4$ structure, but only about half of such runs reach the $n = 4$ structure; the other half freezes in some local minima of the I phase with the structure corresponding to mixture of domains of several phases. Usually they are formed of several large triangles (corresponding to much larger n) surrounded by one or two domains of phases with n smaller than expected in ideal case. Only such a type of domains is obtained for runs with decreasing temperature in the $n = 5$ region; i.e., we do not obtain the ideal $n = 5$ phase at low temperature.

The successful $c(T)$ dependence obtained during runs with decreasing temperature shows that transition from the I phase to the flower phase occurs by abrupt decrease of concentration at T_{c2} almost down to the ground state phase concentration. The "freezing" in domain structure usually occurs without visible change of concentration at T_{c2}. This is illustrated in the inset to Fig. 8 by a run in the $n = 5$ region.

In Figs. 9(a)–9(d) we present the snapshots just above and below the T_{c2} point for successful transitions into the $n = 3$ and 4 phases obtained in simulations with decreasing temperature. The snapshots for transition into the $n = 3$ phase are taken at

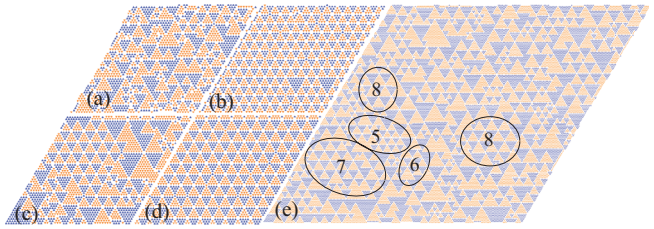

FIG. 9. (Color online) Snapshots just above and below T_{c2} for runs with T-down. The $n = 3$ phase region ($\mu/\epsilon_1 = 0.9$): (a) $k_BT/\epsilon_1 = 0.36$ and (b) 0.34; the $n = 4$ phase region ($\mu/\epsilon_1 = 0.85$): (c) $k_BT/\epsilon_1 = 0.308$ and (d) 0.300. The run to $n = 5$ is represented by a low-temperature ($k_BT/\epsilon_1 = 0.216$) snapshot (e) of a frozen I phase obtained for $180\sqrt{3} \times 180\sqrt{3}$ lattice at $\mu/\epsilon_1 = 0.8$. Some larger domains of different structures in (e) are indicated by circles.

two close temperature points, but the difference in structures of I (a) and $n = 3$ (b) phases is still visible. The process of transition to the $n = 4$ phase is already started at $k_BT/\epsilon_1 = 0.308$ (c) and manifests itself by domains of both I and $n = 4$ phases. The transition is finished with a very small decrease of temperature down to k_BT/ϵ_1=0.300 when an ideal $n = 4$ structure is abruptly established (d). Though, we did not obtain the graduation to the ideal $n = 5$ phase for runs with decreasing temperature, we used to obtain such domains in different frozen I-phase structures. We do not exclude the possibility that successful runs could be possible for very large lattices. The largest one we used in the $n = 5$ phase region ($\mu/\epsilon_1 = 0.8$) had the size $180\sqrt{3} \times 180\sqrt{3}$, and the I phase frozen at low temperature had the domains of the $n = 5$–8 phases [see Fig. 9(e)].

C. $n = \infty$

We do not obtain the T_{c2} point and ideal flower structure for phases with $n > 5$ ($\mu/\epsilon_1 < 0.84$) in simulations with decreasing temperature, but the transition to the I phase at T_{c1} is clearly seen, and T_{c1} increases with increase of n. Neither energy nor concentration experiences any abrupt changes related to formation of the flower phases. But the domains of the I phase are formed, and the system gradually freezes in one of multiple local minima of the I phase.

In the superflower region (as well as for any very large n) the difference between the results of temperature up and down simulations vanishes, and the former does not show any hint of anomaly at T_{c2}. In our calculations the superflower phase, which exists below $\mu/\epsilon_1 = 0.6$, at low temperature always chooses the configuration characterized by several huge domains as shown in Fig. 10. The phase transition temperature $k_BT_{c1}/\epsilon_1 = 0.58$ at $\mu/\epsilon_1 = 0.6$, and this temperature increases with further decrease of μ.

D. Phase diagrams

The phase (μ, T) diagrams obtained in simulations with decreasing and increasing temperature are presented in Fig. 11. The transition temperature T_{c1} from disordered to $n = 1$ and I phases increases with increase of phase index n, while T_{c2} decreases. Thus, in our model we obtain that the stability of a whole ordered region associated to some n (I phase and n

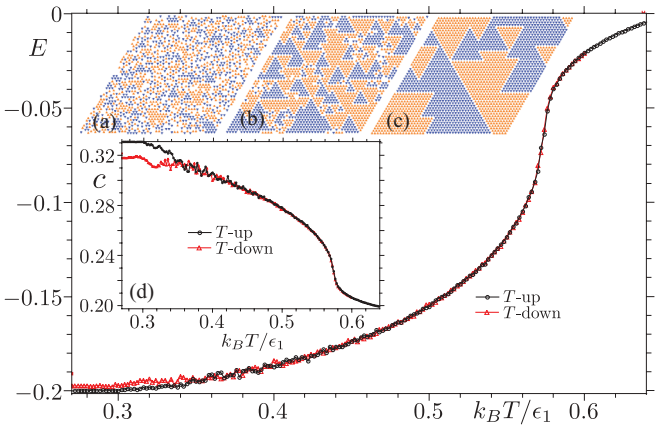

FIG. 10. (Color online) Temperature dependencies of energy and concentration [(d) inset] for $n = \infty$ ($\mu/\epsilon_1 = 0.6$) phase region obtained with increasing (T-up) and decreasing (T-down) temperature. Snapshots in insets are (a) $k_BT/\epsilon_1 = 0.6$, (b) 0.5, and (c) 0.2.

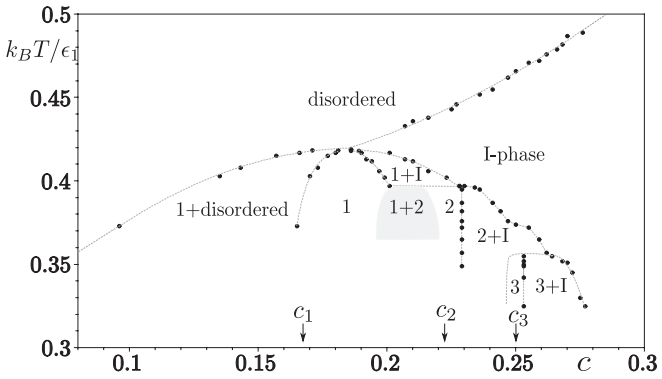

FIG. 12. Phase diagram in (c,T) coordinates. Dashed lines without dots close to $n = 2$ and 3 phase regions are our conjectures. The two-phase $1+2$ area (shown in gray) is obtained from $c(\mu)$ calculations between $k_BT/\epsilon_1 = 0.4$ and 0.37. The accuracy of T_{c2} points is not shown here for convenience, but the error bars do not exceed $k_BT/\epsilon_1 = \pm 0.01$.

phase) increases, but the stability of the ideal flower phase itself decreases with increase of n.

There are two interesting features of the diagram obtained in simulations with decreasing temperature [Fig. 11(a)]. The first is related to the mentioned fact that we cannot obtain the T_{c2} point for $n > 4$. The second might be seen comparing the ranges of chemical potential corresponding to some flower phase obtained in ground state and finite temperature calculations. The phases with smaller index $n = 1$ and 2 "misappropriate" part of the μ range corresponding to the neighboring $n+1$ phase as known from the ground state calculations; e.g., in MC calculations the $n = 1$ phase exists

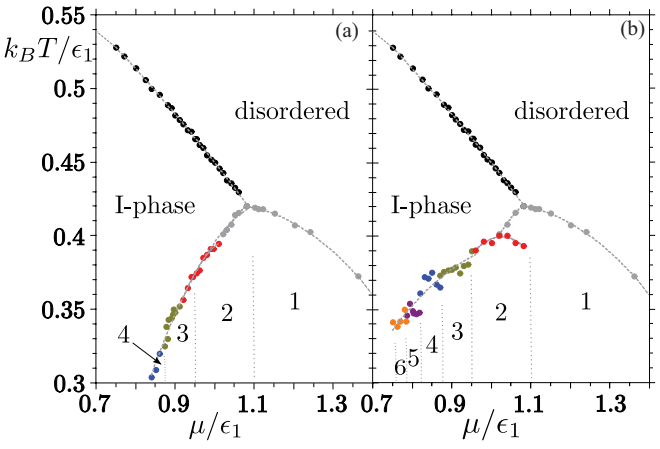

FIG. 11. (Color online) Phase diagram in (μ,T) coordinates obtained with (a) decreasing and (b) increasing temperature. Dots are simulation results. In the electronic version the color of dots mark transitions to or from different phases: black (I phase), gray ($n = 1$), red ($n = 2$), brown ($n = 3$), blue ($n = 4$), purple ($n = 5$), and orange ($n = 6$). Dashed vertical lines and numeration of flower phases at lower temperature indicate the ground state limits of flower phases. Dashed vertical lines, downward arrows, and numeration of phases close to the T_{c2} point in (a) are given to demonstrate the difference between the finite temperature and ground state results. The accuracy of T_{c2} points is not shown here for convenience, but the error bars do not exceed $k_BT/\epsilon_1 = \pm 0.01$.

down to $\mu/\epsilon_1 = 1.0$ instead of 1.1 and the $n = 2$ phase down to $\mu/\epsilon_1 = 0.90$ instead of 0.95.

In Fig. 11(b) the bell-shaped tops of $n = 1$, 2, and partly 3 phase might be distinguished in simulations with increasing temperature. The results for transitions to other phases also imply some kind of plateau inside the ranges of μ associated to that particular phase. For simulations with increasing temperature we also managed to find the sequence of phase transitions at finite temperature, $2 \to 1 \to \mathrm{I} \to$ disordered and $3 \to 2 \to \mathrm{I} \to$ disordered, at the borders of $n = 1-2$ and $n = 2-3$ phases, respectively.

Using the results of temperature dependencies of molecular concentration with decreasing temperature we obtained the phase (c,T) diagram including the interval of concentrations of the first three flower phases (Fig. 12). It is seen that the flower phases in their pure form might be obtained at concentrations corresponding to (or rather close to) stoichiometric concentrations of the phases $n = 1$, 2, and 3. The top of the $n = 1$ phase is a bit shifted towards higher concentration due to the tendency of this phase at finite temperature to exist at such values of μ, which (according to the ground state results) have to belong to the $n = 2$ phase.

The model allows for large two-phase regions between neighboring phases. We found the two-phase regions, $1+\mathrm{I}$, $2+\mathrm{I}$, and $3+\mathrm{I}$, which separate pure flower phases from the I phase. In $c(T)$ calculations we did not find the two-phase region $1+2$, but the data from $c(\mu)$ calculations clearly imply that it should exist at temperature values a bit lower than that of the $1+\mathrm{I}$ region. Therefore we added this region (shadowed gray) into the (c,T) diagram of Fig. 12.

E. Metastable structures

The (μ,T) phase diagram might be also obtained from $c(\mu)$ dependencies at different values of temperature. These calculations allow to find the structure existing at concentrations in between the stoichiometric concentrations of two phases, e.g., $n = 1$ and 2. The jump in concentration $c_2(T) - c_1(T)$ at some value of μ_c indicates the existence of a two-phase (phase separation) region; i.e., two phases coexist in between

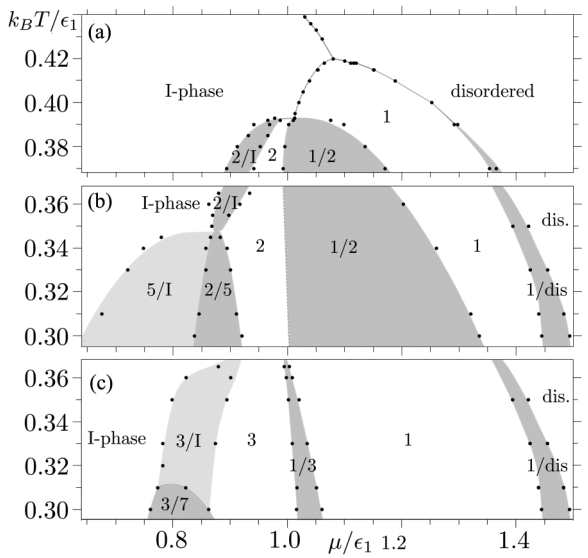

FIG. 13. Phase diagram in (μ,T) coordinates showing stable transitions between 1, 2, and I phases (a) and some metastable transitions between the phases 1 and 3, 2 and 5, 3 and 7 [(b), (c)]. See the text for explanation. Here the areas shaded gray and the denotation A/B indicate $c(\mu)$ hysteresis regions between phases A and B, like those shown in Fig. 14. The accuracy of T_{c2} points is not shown here for convenience, but the error bars do not exceed $k_BT/\epsilon_1 = \pm 0.01$.

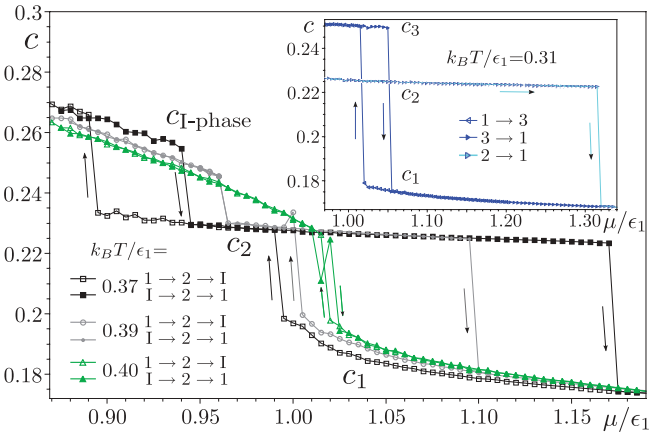

FIG. 14. (Color online) Hysteresis in $c(\mu)$ dependencies between $n = 1$, 2, and I phases corresponding to diagram in Fig. 13(a) and obtained at temperature values below T_{c2} with increasing and decreasing chemical potential. Inset: Illustration of $2 \to 1 \to 3$ transition shown in Figs. 13(b) and 13(c).

$c_1(T)$ and $c_2(T)$ at some particular temperature T (note that this μ_c is not necessarily the one obtained from ground state calculations). Also, the hysteresis is sometimes found [16,35] in $c(\mu)$ dependencies. It defines the stability limits of two phases and usually broadens with decrease of temperature. The "real" μ_c for concentration jump is expected between the range of μ values limited by the hysteresis.

It should be noted that the $c(\mu)$ curves might be a bit misleading in MC calculations at low temperature, since for complicated structures with many local energy minima they tend to demonstrate spurious transitions to metastable structures. On the other hand, it is quite possible that such metastable transitions occur in real experiments.

We performed the $c(\mu)$ calculations with increasing and decreasing chemical potential μ just below T_{c2}. The results entirely based on these calculations are shown in (T,μ) diagrams of Fig. 13. We did not find any metastabilities in $n = 1$ and 2 phase regions at $k_BT_{c2}/\epsilon_1 \geqslant 0.37$. This statement is based on a feedback of our results: The transition between two neighboring phases is reversible and does not depend on choice of initial phase for hysteresis calculations. The $c(\mu)$ behavior in this temperature range is shown in Fig. 14, and the results are generalized in (μ,T) diagram in Fig. 13(a), where the hysteresis regions are shaded gray. In between $k_BT_{c2}/\epsilon_1 = 0.37$ and 0.4 there exist pure structures $n = 1$ and 2 and hysteresis regions between phases $n = 1$ and 2, as well as $n = 2$ and I phase. The diagram basically corresponds to that obtained in Fig. 11. It should be noted that the initial phase for $c(\mu)$ simulation is always chosen in accordance with the μ limits defined by the ground state calculations.

The $c(\mu)$ dependencies at lower values of temperature, $k_BT_{c2}/\epsilon_1 < 0.37$, are more complicated, and, we believe, the metastable structures start to appear. The phases participating in hysteresis depend on which phase was used as the initial one for simulation. The hysteresis is seen not only between neighboring phases $n = 1$ and 2, but between $n = 1$ and 3 or $n = 2$ and 5 or even $n = 3$ and 7. At $k_BT_{c2}/\epsilon_1 < 0.37$ we obtain two scenarios which are demonstrated in Figs. 13(b) and 13(c), respectively. In Fig. 13(b) we show the situation, when the initial phase for $c(\mu)$ calculations is the $n = 2$ structure in its ground state limits. With decrease of μ, the transition (hysteresis) between $n = 2$ and 5 phases is obtained followed by the hysteresis between $n = 5$ and I phases. With increase of μ, the $n = 2$ phase transits into the $n = 1$ phase and further to the disordered phase. But the reverse transition at that temperature from the $n = 1$ phase proceeds according to the scenario shown in Fig. 13(c). With decreasing μ, the $c(\mu)$ dependence demonstrates the jump from concentration characteristic to $n = 1$ phase to that of $n = 3$ phase, avoiding the "step" of the $n = 2$ phase (see inset in Fig. 14). The transition into the $n = 3$ phase is further followed by the transition either to I or $n = 7$ phase.

On one hand, we can attribute such type of behavior to a well-known inability of the MC method to deal with the first-order phase transitions and phase separation at lower temperature when the dynamics of diffusion is hindered. This is probably the only point, where approximate methods, the cluster variation method (CVM) [41–43] in particular, still have a certain advantage [44,45] over MC simulations. Unfortunately the chosen clusters even for the smallest flower phases should be quite large in order to obtain reliable results using CVM for this model.

On the other hand, the metastabilities and transitions between non-neighboring phases might be caused by geometrical-structural reasons and therefore might manifest themselves in experiments. In snapshots of our temperature dependencies we have noticed that the flower phase with small index n can successfully form nicely packed domains with structurally related phases n_i according to formula $n_i = (n+1)i - 1$. It means that $n = 1$ phase readily packs with itself and phases $n = 3$, 5, etc.; $n = 2$ with itself and $n = 5$,

8, etc., and $n = 3$ with itself and $n = 7$, 11, etc. [see e.g. the coexistence of domains of $n = 3$ and 7 phases in Fig. 9(b)].

V. DISCUSSION

As a statistical model for studies of self-assembly of TMA molecules, the 2NN-3NN model captures main ordering properties of TMA molecular system and correctly describes the occurrence of flower phases. However, while constructing the model, we deliberately used two important assumptions which allowed to make the model rather simple and solvable. First, the number of possible states of a molecule was restricted to those found in ideal flower structures. Naturally, there are more possible states of the molecule, but they usually play a more important role at higher temperature. Second, by rescaling of the initial lattice, we decreased the number of sites for hopping of the molecule, thus restraining the model and decreasing its number of degrees of freedom. Though these assumptions should not affect low-temperature results, the question might arise how reliable are the results obtained for higher temperature and what is the accuracy of evaluation of phase transition points. In particular, is the abruptness of phase transition at T_{c2} a natural feature or just some artifact of the model? The occurrence of the intermediate phase might be questioned as well.

In principle, the existence of the intermediate phase might be supported by the following argument: As ordering systems the flower phases have very complicated symmetry; therefore some intermediate phase is needed as a prerequisite for flower phase formation. The restriction of the system occurring due to lack of sites for hopping can deform this phase. Therefore it is quite possible that instead of some identifiable long-range ordered intermediate phase we obtain the system of correlated domains lacking long-range order.

Moreover, in such complex systems the two-phase (phase separated) structures with the energy comparable to that of the ideal flower phase might exist at finite temperature. They might be stable and metastable (formed by domains of similar geometry) as shown above. We assume that such mixed phases might have some advantage in energy over the pure phase at finite temperature and be the basic building block for intermediate phase formation. Due to entropy effects and limited lattice sizes this phase has sometimes rather "deformed" structure but still retains some relation to a low-temperature flower phase. Some support for this assumption might be gained from simulations with decreasing temperature when an intermediate phase gradually "freezes" in some local minimum corresponding to deformed form of the mixture of phases [see Fig. 9(e)].

Considering the important issue of reduction of possible sites for molecules diffusion in our model, we must say that in general, this effect decreases the entropy of the system, especially for disordered phases, strengthens ordered phases and, as a result, increases T_c. It is also known [46] that the phase transition temperature slightly increases with the decrease of number of possible states in both ferromagnetic and antiferromagnetic Potts models. The same tendency is seen for a square-lattice Potts model with mixed ferromagnetic and antiferromagnetic interactions [47], which is rather close to the model considered here. Thus, we expect that the phase transition temperature in a model with more states and sites for hopping should be lower than that obtained in our work.

Trying to clarify the finite temperature behavior of the system including the existence of intermediate phase itself, we performed some simulations with a simplified version of more general model. We kept the same number of states, but allowed for a more realistic number of sites for hopping.

As mentioned, in an unscaled model for flower phases on Au(111) two molecules in "tip-to-tip" (dimeric) orientation have their centers $2\sqrt{3}a_{\mathrm{Au}}$ [or equivalently 6NN of Au(111) lattice] apart [27]. It should be expected then, for three molecules of the same orientation forming trimeric trio interaction, to have their centers $3a_{\mathrm{Au}}$ (5NN) apart. Taking into account the values of $a_{\mathrm{Au}} = 0.288$ nm and the radius of TMA molecule ($\sim$0.5 nm), we can easily eliminate 1NN and 2NN intermolecular distances due to exclusion. It is more complicated to evaluate a mutual layout of the molecules at 3NN and 4NN distances. The formation of molecules with 3NN distance in between is clearly excluded for molecules of different orientations and, most likely, for molecules of the same orientation as well. The formation of molecules of the same orientation with 4NN distance in between is quite conceivable, and most such dimers could probably even organize the H bonds. The layout of two molecules of different orientations with 4NN distance in between is also possible for 8 out of 12 neighbors. Some mutual orientations on 4NN even remind one of those of a double row TMA network on Cu(110) [25]. Thus, the general model is too complicated, but we increase the number sites and make it tractable in a following way. Irrespective of orientation, the mutual exclusion of molecules is assumed at 1NN, 2NN, and 3NN distances, and the sites for hopping are provided for molecules 4NN apart assuming though that there is no interaction at this particular distance. The only interactions are dimeric "tip-to-tip" and trimeric trio (for three molecules of the same orientation with carboxylic vertices directed to the center of a common triangle) at 6NN and 5NN distances, respectively. Thus, we use some version of a Lennard-Jones potential with exclusion at 1NN, 2NN, and 3NN, zero interaction at 4NN, and attractions at 5NN and 6NN. All further interactions are neglected.

Preliminary comparison of results for two models revealed some quantitative, rather than qualitative differences. Thus, using the 5NN-6NN model the phase transition temperature from disordered to the honeycomb phase, T_c, indeed decreases by 15%. The intermediate phase for flower phases with $n > 1$ still exists, but the temperature interval of its existence is considerably reduced, mostly due to decrease of T_{c1}. The energy jump at T_{c2} remains abrupt as in the 2NN-3NN model, but the transition at T_{c1} also becomes rather steep. In intermediate phase, existing at temperature which is above the phase transition temperature T_{c2} to flower phases with small $n(< 4)$, the inserts of the honeycomb structure are observed.

In experiments the ordered molecular structures are usually characterized by molecular packing density. Here we use the concentration defined as the coverage of sites occupied by the center of the molecule, the definition usually employed for adatoms on surfaces. Recalculation is possible. It shows that the packing density ρ is a bit higher in our model than in experiment [28], but only for phases with large index n. Taking $a_{\mathrm{Au}} = 0.2885$ nm, the packing density in our model might be

roughly calculated as 0.77, 1.03, and 1.54 molecules/nm^2 for the honeycomb ($n = 1$), flower ($n = 2$), and superflower ($n = \infty$) phases, respectively. The experimental data on Au(111) give $\rho = 0.8$ [27] and 0.85 [28] for the honeycomb, 1.04 [28] for the flower ($n = 2$), and 1.34 [28] for the superflower phase. The corresponding numbers on graphite are $\rho = 0.8$ for the honeycomb and 1.11 molecules/nm^2 for the flower phase [22]. We find this agreement quite satisfactory. The discrepancy of 15% for the superflower phase comes from the fact that in experiment the ratio of distances between two molecules in dimeric and trimeric state is, most likely, closer to 1, while in our model it is $2/\sqrt{3}$.

In conclusion, we proposed and solved the three-state model for ordering of triangular molecules into homologous series of flower phases. Such structures are experimentally observed in self-assembled networks of TMA molecules. The model has two types of interactions which mimic the H-bond interactions of TMA molecules: the dimeric "tip-to-tip" interaction and the trimeric trio interaction of three molecules. The former is defined for two molecules of different states separated by the third neighbor distance of triangular lattice. The latter is defined for three molecules of the same state forming an equilateral triangle to the center of which the carboxylic "leg" of each molecule is directed. The side of the triangle corresponds to second neighbor distance of the lattice. We analytically obtained the ground state phase diagram of the model. Simulation of thermodynamics by the Monte Carlo method revealed that phase transition into the flower phase is mediated by the intermediate phase. This structure with triangular domains of different sizes has no long-range order, but still retains some relation to the neighboring flower phases. Possibly this phase is required as a preparatory stage to formation of the flower structure. At stoichiometric concentrations the ideal flower phases are obtained. As a rule, the less dense the flower structure, the more easily it is accessible in simulations. Denser structures often "freeze" in some local energy minimum with the structure corresponding to mixture of domains of several phases. This could explain why only the first members of homologous series are rather successfully found in experiments. The results also imply that between stoichiometric concentrations of two flower phases, the phase separation of these phases might exist, including the possibility of metastable ordered formations.

ACKNOWLEDGMENTS

We are grateful to S. Lapinskas, V. Petrauskas, K. Pyragas, and M. Šimėnas for discussions. This work is being funded by European Union Structural Funds project "Postdoctoral Fellowship Implementation in Lithuania" (No. VP1-3.1-ŠMM-01-V-02-004).

[1] Y. L. Huang, W. Chen, H. Li, J. Ma, J. Pflaum, and A. T. S. Wee, Small **6**, 70 (2010).
[2] L. Bartels, Nature Chem. **2**, 87 (2010).
[3] S. M. Lindsay and M. A. Ratner, Adv. Mater. **19**, 23 (2007).
[4] Z. Liu, A. A. Yasseri, J. S. Lindsey, and D. F. Bocian, Science **302**, 1543 (2003).
[5] J. E. Green, J. W. Choi, A. Boukai, Y. Bunimovich, E. Johnston-Halperin, E. DeIonno, Y. Luo, B. A. Sheriff, K. Xu, Y. S. Shin, H.-R. Tseng, J. F. Stoddart, and J. R. Heath, Nature (London) **445**, 414 (2007).
[6] T. Kondo and K. Uosaki, J. Photochem. Photobiol. C: Photochem. Rev. **8**, 1 (2007).
[7] M. S. Kang, S. H. Kang, H. Ma, K.-S. Kim, and Alex K.-Y. Jen, J. Power Sources **160**, 711 (2006).
[8] F. I. Bohrer, C. N. Colesniuc, J. Park, M. E. Ruidiaz, I. K. Schuller, A. C. Kummel, and W. C. Trogler, J. Am. Chem. Soc. **131**, 478 (2009).
[9] S. P. Jiang, L. Li, Z. Liu, M. Pan, and H. L. Tang, Electrochem. Solid State Lett. **8**, A574 (2005).
[10] B. Bhushan, Philos. Trans. R. Soc. **366**, 1499 (2008).
[11] E. Ostuni, L. Yan, and G. M. Whitesides, Colloids Surfaces B **15**, 3 (1999).
[12] M. Kind and C. Woell, Prog. Surf. Sci. **84**, 230 (2009).
[13] S. Stepanow, M. Lingenfelder, A. Dmitriev, H. Spillmann, E. Delvigne, N. Lin, X. Deng, C. Cai, J. V. Barth, and K. Kern, Nature Mat. **3**, 229 (2004).
[14] J. M. MacLeod, O. Ivasenko, D. F. Perepichka, and F. Rosei, Nanotechnology **18**, 424031 (2007).
[15] S. Berner, M. de Wild, L. Ramoino, S. Ivan, A. Baratoff, H.-J. Guentherodt, H. Suzuki, D. Schlettwein, and T. A. Jung, Phys. Rev. B **68**, 115410 (2003).
[16] V. Petrauskas, S. Lapinskas, and E. E. Tornau, J. Chem. Phys. **120**, 11815 (2004).
[17] M. A. Osipov and J. Stelzer, Phys. Rev. E **67**, 061707 (2003).
[18] G. Pawin, K. L. Wong, K.-Y. Kwon, and L. Bartels, Science **313**, 961 (2006).
[19] M. O. Blunt, J. C. Russell, M. del Carmen Giménez-López, J. P. Garrahan, X. Lin, M. Schroeder, N. R. Champness, and P. H. Beton, Science **322**, 1077 (2008).
[20] U. K. Weber, V. M. Burlakov, L. M. A. Perdigao, R. H. J. Fawcett, P. H. Beton, N. R. Champness, J. H. Jefferson, G. A. D. Briggs, and D. G. Pettifor, Phys. Rev. Lett. **100**, 156101 (2008).
[21] S. Griessl, M. Lackinger, M. Edelwirth, M. Hietschold, and W. M. Heckl, Single Mol. **3**, 25 (2002).
[22] M. Lackinger, S. Griessl, W. M. Heckl, M. Hietschold, and G. W. Flynn, Langmuir **21**, 4984 (2005).
[23] K. G. Nath, O. Ivasenko, J. M. MacLeod, J. A. Miwa, J. D. Wuest, A. Nanci, D. F. Perepichka, and F. Rosei, J. Phys. Chem. C **111**, 16996 (2007).
[24] N. T. N. Ha, T. G. Gopakumar, R. Gutzler, M. Lackinger, H. Tang, and M. Hietschold, J. Phys. Chem. C **114**, 3531 (2010).
[25] T. Classen, M. Lingenfelder, Y. Wang, R. Chopra, C. Virojanadara, U. Starke, G. Costantini, G. Fratesi, S. Fabris, S. de Gironcoli, S. Baroni, S. Haq, R. Raval, and K. Kern, J. Phys. Chem. A **111**, 12589 (2007).

[26] A. Dmitriev, N. Lin, J. Weckesser, J. V. Barth, and K. Kern, J. Phys. Chem. B **106**, 6907 (2002).
[27] Z. Li, B. Han, L. J. Wan, and T. Wandlowski, Langmuir **21**, 6915 (2005).
[28] Y. C. Ye, W. Sun, Y. F. Wang, X. Shao, X. G. Xu, F. Cheng, J. L. Li, and K. Wu, J. Phys. Chem. C **111**, 10138 (2007).
[29] P. Pasini, C. Chiccoli, and C. Zannoni, *Advances in the Computer Simulation of Liquid Crystals* (Kluwer, Dordecht, 2000).
[30] K. Binder and W. Paul, Macromolecules **41**, 4537 (2008).
[31] J. Higo, S. Endo, and K. Nagayama, Chem. Phys. Lett. **198**, 300 (1992).
[32] A. Šarlah, E. Frey, and T. Franosch, Phys. Rev E **75**, 021402 (2007); A. Šarlah, T. Franosch, and E. Frey, Phys. Rev Lett. **95**, 088302 (2005).
[33] E. Bianchi, J. Largo, P. Tartaglia, E. Zaccarelli, and F. Sciortino, Phys. Rev. Lett. **97**, 168301 (2006).
[34] S. Fortuna, D. L. Cheung, and A. Troisi, J. Phys. Chem. B **114**, 1849 (2010).
[35] T. Misiūnas and E. E. Tornau, J. Phys. Chem. B **116**, 2472 (2012).
[36] M. Korth, J. Chem. Theory Comput. **6**, 3808 (2010).
[37] V. Petrauskas (private communication).
[38] M. S. S. Challa, D. P. Landau, and K. Binder, Phys. Rev. B **34**, 1841 (1986).
[39] J. Lee and J. M. Kosterlitz, Phys. Rev. B **43**, 3265 (1991).
[40] S. Sinha and S. K. Roy, Phys. Rev. E **81**, 022102 (2010).
[41] R. Kikuchi, Phys. Rev. **81**, 988 (1951); J. Chem. Phys. **19**, 1230 (1951).
[42] T. Morita, J. Phys. Soc. Jpn. **12**, 753 (1957).
[43] V. Zubkus and S. Lapinskas, J. Phys. Cond. Matter **2**, 1753 (1990).
[44] V. E. Zubkus, E. E. Tornau, S. Lapinskas, and P. J. Kundrotas, Phys. Rev. B **43**, 13112 (1991).
[45] G. Grigelionis, S. Lapinskas, A. Rosengren, and E. E. Tornau, Physica C **242**, 183 (1995).
[46] F. Y. Wu, Rev. Mod. Phys. **54**, 235 (1982).
[47] W. Kinzel, W. Selke, and F. Y. Wu, J. Phys. A **14**, L399 (1981).